LONG TERM ANALYSIS OF STRONG NON-LINEAR DEFORMATIONS INDUCED BY COAL MINING USING THE SBAS TECHNIQUE

Kanika Goel, Nico Adam, Christian Minet

Remote Sensing Technology Institute (IMF), German Aerospace Center (DLR), Oberpfaffenhofen, 82234- Wessling, Germany. Email: kanika.goel@dlr.de

ABSTRACT

This paper demonstrates the application of differential interferometric SAR (DInSAR) for monitoring strong non-linear subsidence induced by coal mining. We present eleven years (1993-2004) of deformation estimation results for Gardanne coal mine in France exploiting ERS-SAR data. This coal mine represents a difficult test site for applying C-band Persistent Scatterer Interferometry (PSI) due to strong non-linear motions occurring in the region, low density of persistent scatterers (PSs) and difficult to compensate atmospheric effects. This has been shown in the study conducted by ESA for the PSIC4 project. In fact, Gardanne coal mine is an application test case for the Small Baseline Subset Algorithm (SBAS) which makes use of small baseline highly coherent differential interferograms and focuses on distributed scatterers (DSs). We present here the deformation results obtained for Gardanne coal mine using the SBAS technique.

***Index Terms*—** ERS, Gardanne Coal Mine, Persistent Scatterer Interferometry (PSI), PSIC4 Project, Small Baseline Subset Algorithm (SBAS).

1. INTRODUCTION

Differential Interferometric SAR (DInSAR) is a powerful tool for deformation monitoring of Earth's surface [1]-[3]. Mining induced subsidence is an important area where DInSAR can be applied. In this study, we illustrate the potential of this technique for monitoring strong non-linear subsidence induced by coal mining. We present eleven years (1993-2004) of deformation estimation results for Gardanne coal mine located in Southern France exploiting SAR data acquired by ERS-1 and ERS-2 satellites. The mining started in the 17th century and went on till 2003. Due to the continuous mining, this region experienced strong non-linear subsidence ranging from zero (in stable areas) to a few centimeters per year.

Monitoring the subsidence induced by mining is important for geological and hazard analysis and DInSAR has been used for mapping deformation time series using advanced techniques such as Persistent Scatterer Interferometry (PSI) [4]-[6] and Small Baseline Subset Algorithm (SBAS) [7]-[9]. Gardanne coal mine represents a difficult test case for deformation monitoring using the C-band ERS sensors with 5.6 cm wavelength, a revisit time of 35 days and a maximum detectable deformation rate of 14.6 cm/year in radar's line-of-sight (LOS). Reasons include the strong non-linear motion occurring in the region, low density of persistent scatterers (PSs) present in this rural area and difficult to compensate atmospheric effects. C-band PSI is difficult to implement as many points experienced fast subsidence in the considered time period with sudden non-linear movements and it is difficult to fit a model to the actual deformations. This has been demonstrated in the study conducted by the European Space Agency (ESA) for PSIC4 (PSI Codes Cross-Comparison and Certification for Long-Term Differential Interferometry) project [10], [11]. As a matter of fact, Gardanne coal mine is an application test case for the SBAS technique which makes use of small baseline differential interferogram subsets. Using this approach, non-linear deformation can be estimated without any modelling and prior knowledge even in non-urban areas where PS density is low and temporal decorrelation is faster.

We present the deformation results obtained using SBAS for Gardanne coal mine and show visualizations of the geocoded deformation time series in Google Earth. The mapped subsidence compares well with levelling data used in the PSIC4 project. The results illustrate that SBAS is well suited for monitoring mining induced strong non-linear deformations and similar applications in rural areas as compared to PSI.

2. TEST SITE

Gardanne coal mine is located in Southern France between Aix-en-Provence and Marseille, close to the town of Gardanne, as shown in Fig. 1. Marseille - Aix-en-Provence is the second largest urban area in France (with approximately 1.47 million people) and land deformation monitoring is important for risk analysis.

As mentioned in the PSIC4 project report [10], during the considered time period (1993-2004), the mining was based on the longwall technique which resulted in a faster and larger deformation as compared to the room and pillar techniques used previously in this area. During this time, the mining panels were located at a depth of 600 - 1100 meters, with a width of about 250

Proc. 'Fringe 2011 Workshop', Frascati, Italy, 19–23 September 2011 (ESA SP-697, January 2012)

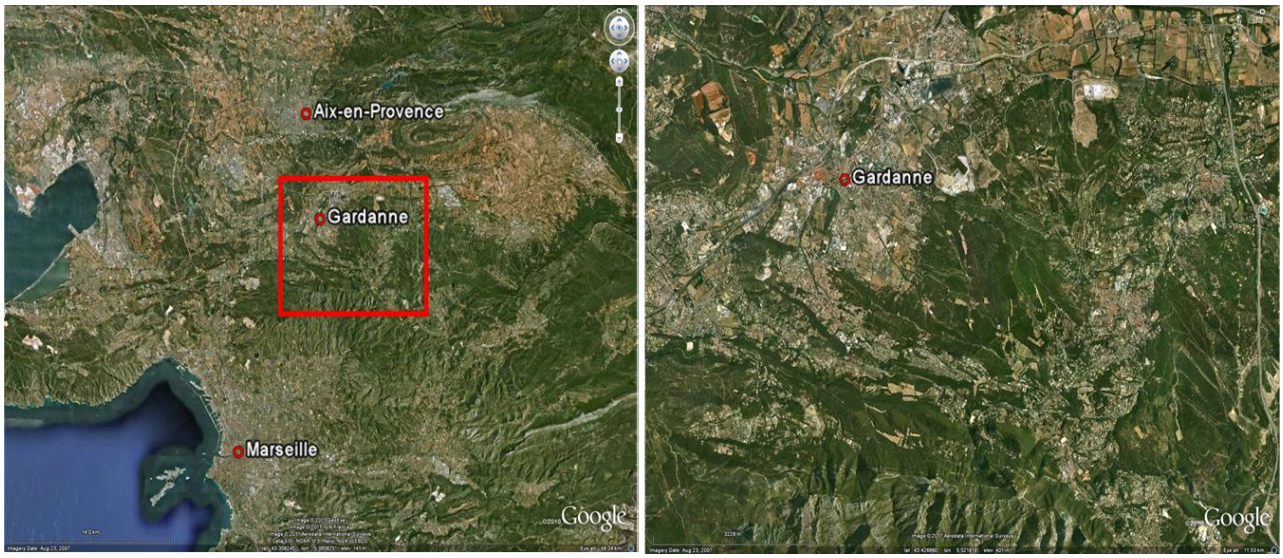

(a) (b)

Figure 1. (a) shows the location of Gardanne coal mine (enclosed in red) in Google Earth, (b) is a zoom-in of the red rectangle in (a).

meters. The thickness of the coal layers ranged between 2 - 3 meters.

Based on the analysis of levelling data, the deformation field is characterised in the PSIC4 report as follows. 70% of the subsidence for a point occurs within the first 3 months of arrival of the mining works and the point becomes stable after 2 years. However, if several mining works overlap, the point continues to subside for more than 2 years.

3. METHODOLOGY

We have used the SBAS technique for generating the deformation time series in radar's LOS for Gardanne coal mine. It focuses on a distributed scattering model and uses small baseline differential interferograms. The SBAS technique has been described in detail in [7], however, we briefly describe the basic concepts here.

We start with a set of $N+1$ coregistered single look complex (SLC) SAR images. We have used 72 ERS images from 30 June, 1993 to 26 June, 2004 in our case. Fig. 2 (a) shows Gardanne's mean amplitude image. The coregistered images are used for generation of M multilooked small baseline differential interferograms. We have generated 165 interferograms based on spatial baseline threshold of 150 m and maximum temporal baseline of 700 days. We performed a complex multilooking with 4 looks in the range direction and 20 looks in the azimuth direction, so that the phase noise is reduced and also, we get approximately square pixels of about 80 meters in both directions. Fig. 2 (b) shows a small baseline differential interferogram of Gardanne, wherein, we can clearly see the deformation fringes. Use of small spatial (perpendicular) baseline limits spatial decorrelation thus providing spatially dense deformation maps, but could result in separation of the interferograms into different subsets in the baseline-time domain. SBAS can link the independent subsets using Singular Value Decomposition (SVD) provided that the subsets overlap in time, as described later in this section. This increases the temporal sampling rate. Fig. 3 shows the baseline-time plot for Gardanne, where, each dot corresponds to a SAR image and each line corresponds to an interferogram.

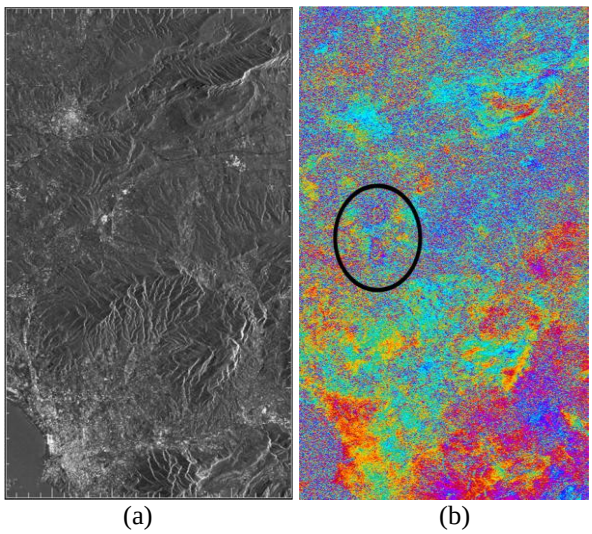

(a) (b)

Figure 2. (a) is Gardanne's mean amplitude ERS-SAR image, (b) is a corresponding small baseline differential interferogram (deformation fringes encircled in black).

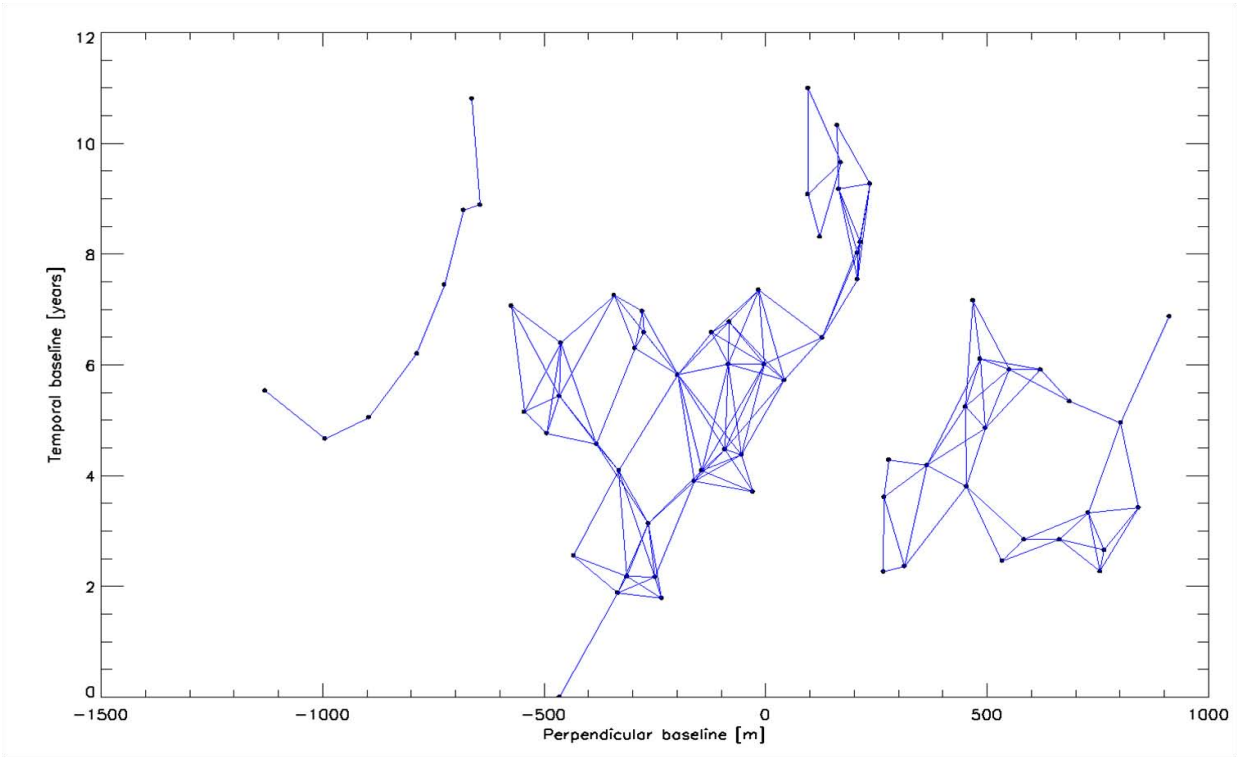

Figure 3. Baseline-time plot for Gardanne, each dot corresponds to a SAR image and each line corresponds to an interferogram. 72 ERS images were used to generate 165 differential interferograms based on spatial (perpendicular) baseline threshold of 150 m and temporal baseline threshold of 700 days.

Next, pixels are identified that exhibit high coherence in all the interferograms and the SBAS approach is applied only to those pixels. For Gardanne, we have used pixels that have an average coherence of at least 0.3. The covariance matrix is shown in Fig. 4.

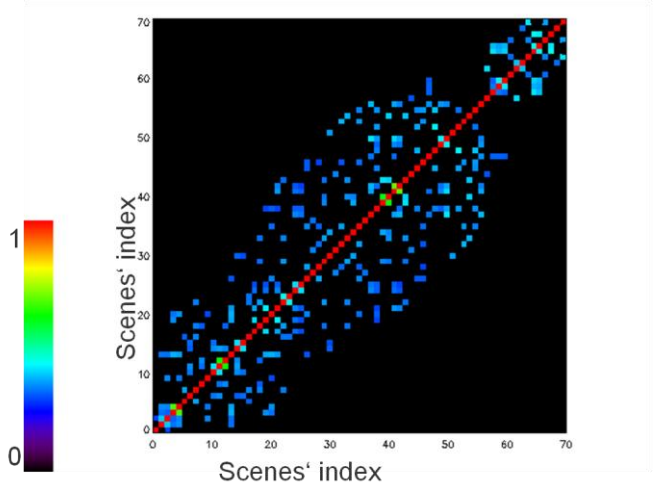

Figure 4. Covariance matrix for Gardanne. It shows the average coherence of the small baseline interferometric pairs used in the SBAS processing.

Subsequently, each of the differential interferograms are unwrapped and all coherent pixels are referenced to one pixel which has a high coherence and a known deformation. The unwrapped differential phase for a coherent pixel in interferogram j, generated by combining SAR images acquired at times t_m (master) and t_s (slave), is given by:

$$\begin{aligned}\delta\phi_j &= \phi(t_m) - \phi(t_s) \\ &\approx \frac{4\pi}{\lambda}[d(t_m) - d(t_s)] \\ &+ \frac{4\pi}{\lambda}\frac{B_{\perp j}\Delta z}{r\sin\theta} \\ &+ [\phi_{atm}(t_m) - \phi_{atm}(t_s)] \\ &+ \Delta n_j ; \forall j = 0,...,M\end{aligned} \quad (1)$$

where, $\phi(t_m)$ and $\phi(t_s)$ are the phases of the coherent pixel at times t_m and t_s respectively, λ is the transmitted radar wavelength, $d(t_m)$ and $d(t_s)$ are the LOS cumulative deformations of the pixel at times

t_m and t_s respectively referenced to the first image i.e. $d(t_0)=0$, $B_{\perp j}$ is the spatial baseline for interferogram j, Δz is the error in the digital elevation model (DEM) used during the differential interferogram generation, r is the sensor-target distance, θ is the local incidence angle (for flat terrain), $\phi_{atm}(t_m)$ and $\phi_{atm}(t_s)$ are the atmospheric phase components for the pixel at times t_m and t_s respectively and finally, Δn_j is the phase contribution due to decorrelation and other noise sources for interferogram j. For coregistration and DInSAR processing, we have employed DLR's operational PSI-GENESIS processor [12], [13]. The coregistration module of the processor uses a geometry based algorithm which utilizes precise orbits and a digital elevation model (DEM) from SRTM. Additionally, we have used this SRTM DEM to remove the topographic phase during the differential interferogram generation. The phase unwrapping is based on the minimum cost flow (MCF) algorithm [14], [15].

After the phase unwrapping step, the low pass (LP) component of the deformation signal and topographic (DEM) error are estimated for each coherent pixel via the least squares solution of the following system of equations:

$$[BM, c]p_c = \delta\phi \tag{2}$$

where, B is the matrix defining the small baseline combinations used, M is the matrix corresponding to a displacement model, c is the vector corresponding to the DEM error, $\delta\phi$ is the vector of unwrapped differential interferometric phase values and p_c is the vector of unknown parameters, namely, the LP component of the deformation signal and topographic error. The estimated DEM error is then subtracted from the unwrapped phase.

The resulting small baseline interferograms form the following linear model for every coherent pixel:

$$Bv = \delta\phi' \tag{3}$$

where, B is the matrix defining the small baseline combinations used as mentioned before, $\delta\phi'$ is the vector of unwrapped differential interferometric phase values after the removal of topographic error and v is the vector of unknown mean phase velocities between time-adjacent acquisitions i.e.:

$$v^T = \left[v_1 = \frac{\phi(t_1)}{t_1 - t_0}, ..., v_N = \frac{\phi(t_N)}{t_N - t_{N-1}} \right] \tag{4}$$

Because of the separation of interferograms into different subsets, the rank of B is $N-L+1$, where $N+1$ is the number of images and L is the number of subsets and thus, Eq. 3 would have infinite solutions. A minimum-norm least squares (LS) solution of Eq. 3 is obtained by using the SVD method as pointed out before in this section [16]. The matrix B is decomposed into matrices U, S and V as follows:

$$B = USV^T \tag{5}$$

where, $S = diag(\sigma_1, ..., \sigma_{N-L+1}, 0, ..., 0)$, σ_i being the singular values. The estimate $\hat{v}$ is then given by:

$$\hat{v} = VS^+U^T\delta\phi \tag{6}$$

where, $S^+ = diag(1/\sigma_1, ..., 1/\sigma_{N-L+1}, 0, ..., 0)$. An additional integration step gives the solution ϕ. It is to be noted that non-linear deformation can be estimated without any modeling and prior knowledge using the SVD.

However, taking Eq. 1 into consideration, the solution also includes decorrelation and atmospheric effects. Though the decorrelation phenomena are mitigated by using small baseline differential interferograms and performing multilooking, atmospheric effects have to be removed. For estimating the atmospheric effects, a LP filtering is performed in the 2D spatial domain after removing the LP deformation estimated via (2), followed by a high pass (HP) filtering in the time domain, since the atmospheric phase component exhibits a high spatial correlation but a low temporal correlation. This operation is similar to the PS approach for removing the atmospheric phase screen [4].

Finally, the estimated phase signal after removal of the atmospheric component is converted into a displacement signal by multiplying with the factor $\lambda/4\pi$, as given in Eq. 1.

4. RESULTS

In this section, we present results from applying the SBAS approach on Gardanne ERS-SAR dataset. The eleven years (1993-2004) deformation estimates for Gardanne coal mine have been geocoded and visualized in Google Earth as shown in Fig. 5.

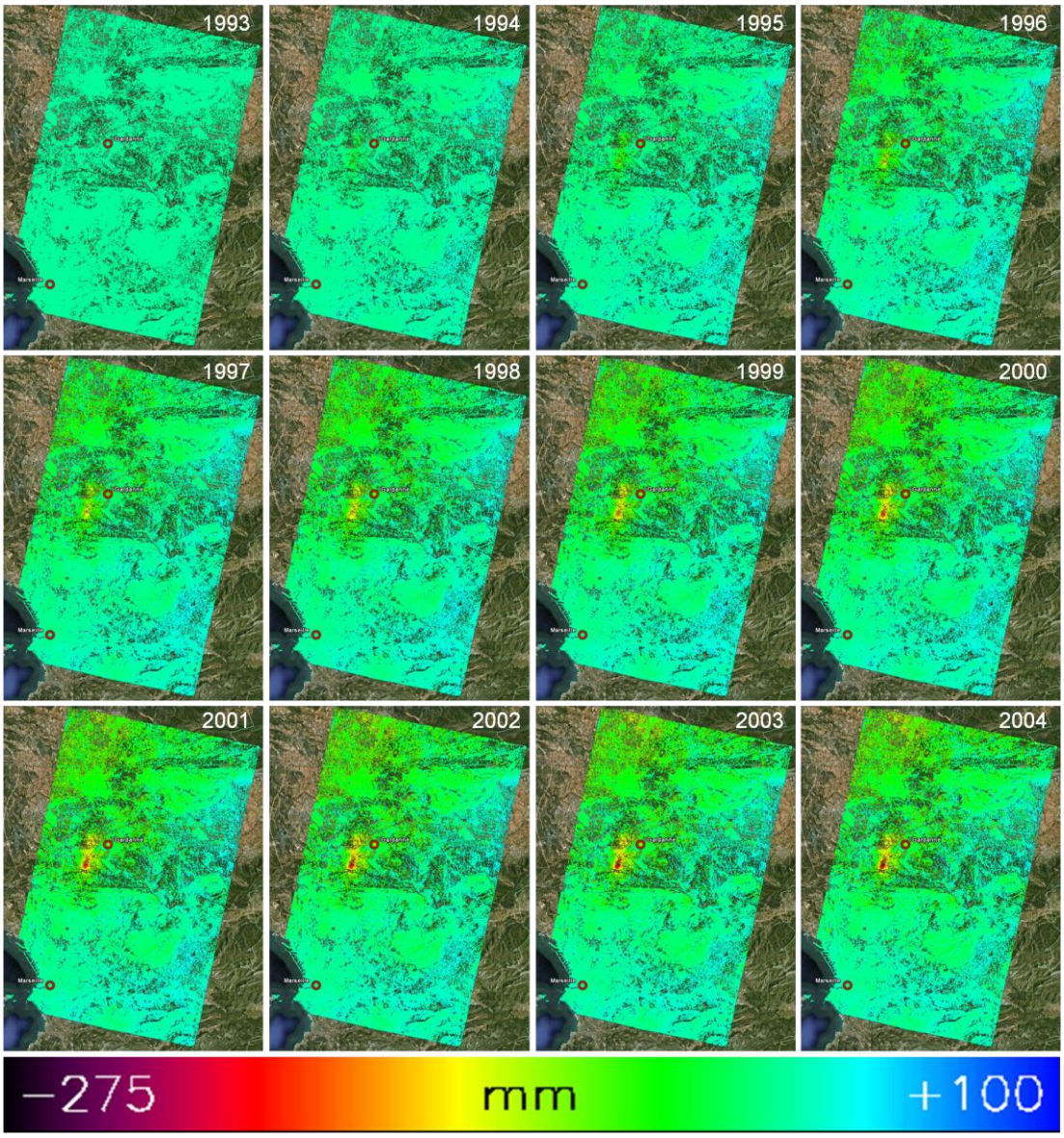

Figure 5. Eleven years (1993-2004) deformation estimates for Gardanne coal mine.

The surface deformation estimates show two subsidence bowls (one having a larger deformation than the other and also covering a larger area). The cumulative deformation is largest in the center of the bowls and gradually decreases as we go away from the center. A maximum of 273.5 mm of cumulative deformation from 1993-2004 has been measured as shown in Fig. 6.

We compared our results with the geodetic levelling results used in PSIC4 project [10], [11] and a visual assessment showed that largely the same areas are subsiding in the considered time period with comparable subsidence patterns. However, a direct comparison is not possible because of different spatial and temporal sampling of the levelling points. Nonetheless, the deformation patterns look similar. In addition, the density of points processed for Gardanne using SBAS is much higher as compared to PSI because SBAS focuses on distributed scatterers (DSs).

5. CONCLUSION

We have demonstrated the applicability of SBAS technique for long term mapping of fast non-linear deformations in rural areas, as compared to PSI. We monitored subsidence for Gardanne coal mine in France by analyzing 72 ERS-SAR images in the time period 1993-2004. SBAS is a promising technique for monitoring mining subsidence and similar applications, and the results can be used for further geological and risk analysis. Future work can concentrate on further comparisons with the geodetic measurements. Furthermore, SBAS can take benefit from adaptive

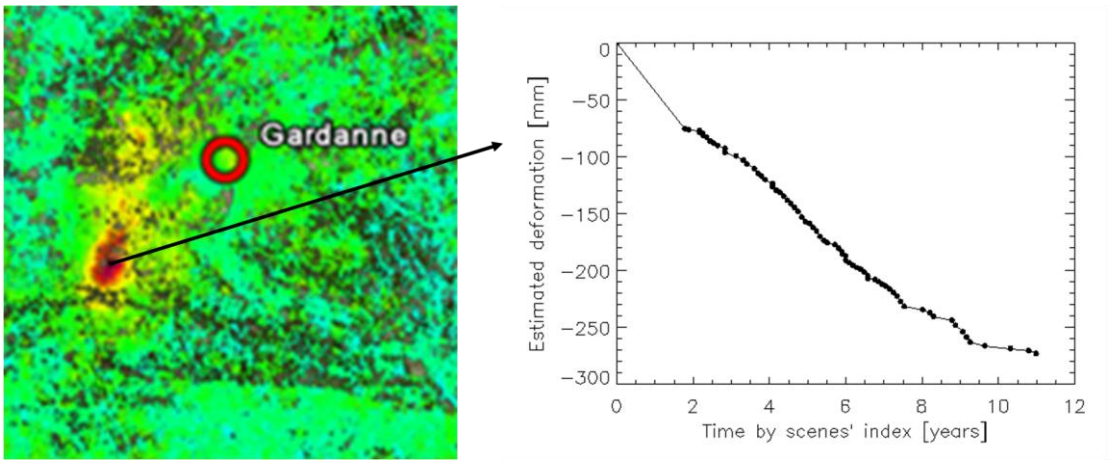

Figure 6. Cumulative deformation of Gardanne from 1993-2004 consisting of two subsidence bowls. A maximum of 273.5 mm of cumulative deformation has been measured.

spatial phase filtering for better estimation of differential interferometric phase and coherence [17].

6. ACKNOWLEDGEMENT

We would like to thank ESA for providing the ERS-SAR data for Gardanne.

7. REFERENCES

1. Massonnet, D., Rossi., M., Carmona, C., Ardagna, F., Peltzer, G., Feigl, K. & Rabaute, T. (1993). The displacement field of the Landers earthquake mapped by radar interferometry. *Nature*, vol. 364, pp. 138–142.

2. Massonnet, D. & Arnaud, A. (1995). Deflation of Mount Etna monitored by space radar interferometry. *Nature*, vol. 375, pp. 567-570.

3. Strozzi, T., Wegmüller, U., Tosi, L., Bitelli, G. & Spreckels, V. (2001). Land subsidence monitoring with differential SAR interferometry. Photogrammetric Engineering and Remote Sensing, 67, 11, 1261–1270.

4. Ferretti, A., Prati, C. & Rocca, F. (2001). Permanent scatterers in SAR interferometry. *IEEE TGARS*, vol. 39, no. 1, pp. 8-20.

5. Adam, N., Eineder, M., Yague-Martinez, N. & Bamler, R. (2008). High resolution interferometric stacking with TerraSAR-X. In: *Proc.IGARSS*, Boston.

6. Gernhardt, S., Adam, N., Eineder, M. &Bamler, R. (2010). Potential of very high resolution SAR for persistent scatterer interferometry in urban areas. *Annals of GIS*, vol. 16, issue 2, pp. 103-111.

7. Berardino, P., Fornaro, G., Lanari, R. & Sansosti E. (2002). A new algorithm for surface deformation monitoring based on small baseline differential SAR interferograms. *IEEE TGARS*, vol. 40, no. 11, p. 2375.

8. Casu, F., Manzo, M. & Lanari, R.. (2006). A quantitative assessment of the SBAS algorithm performance for surface deformation retrieval from DInSAR data. *Remote Sens. Environment.*, vol. 102, p. 195.

9. Lanari, R., Casu, F., Manzo, M., Zeni, G., Berardino, P., Manunta, M. & Pepe, A. (2007). An overview of the small baseline subset algorithm: A DInSAR technique for surface deformation analysis. *Pure Appl. Geophys.*, vol. 164, p. 637.

10. Raucoules, D., Bourgine, B., de Michele, M., Le Cozanet, G., Closset, L., Bremmer, C., Veldkamp, H., Tragheim, D., Bateson, L., Crosetto, M. & Agudo, M. (2007). Persistent Scatterers Interferometry Independent Validation and Intercomparison of Results – Final Report. *BRGM* / RP-55649-FR.

11. Raucoules, D., Bourgine, B., de Michele, M., Le Cozanet, G., Closset, L., Bremmer, C., Veldkamp, H., Tragheim, D., Bateson, L., Crosetto, M., Agudo, M. & Engdahl, M. (2009). Validation and intercomparison of Persistent Scatterers Interferometry: PSIC4 project results. *Journal of Applied Geophysics*, vol. 68, issue 3, pp. 335-347.

12. Adam, N., Kampes, B., Eineder, M., Worawattanamateekul, J. & Kircher, M. (2003). The development of a scientific permanent scatterer system. *ISPRS Hannover Workshop*, Inst. for Photogramm. and Geoinf., Hannover, Germany.

13. Adam, N., Kampes, B. & Eineder, M. (2005). Development of a scientific permanent scatterer system: Modifications for mixed ERS/ENVISAT time series. *Eur. Space Agency Spec. Publ.*, ESA SP-572, p. 457.

14. Constantini, M. (1998). A novel phase unwrapping method based on network programming. *IEEE TGARS*, vol. 36, no. 3, pp. 813-821.

15. Eineder, M., Hubig, M. & Milcke, B. (1998). Unwrapping large interferograms using the minimum cost flow algorithm. In: *Proc. IGARSS*, Seattle.

16. Golub, G.H. & Loan, C.F.V. (1996). *Matrix Computations*, 3rd ed. Baltimore: John Hopkins University Press.

17. Goel, K. & Adam, N. (2011). High resolution differential interferometric stacking via adaptive spatial phase filtering. In: *Proc. IGARSS*, Vancouver.